Acta Crystallographica Section B
Structural Science
ISSN 0108-7681

Large, larger, largest – a family of cluster-based tantalum copper aluminides with giant unit cells. II. The cluster structure

Matthias Conrad,[a] Bernd Harbrecht,[a] Thomas Weber,[b] Daniel Y. Jung[b] and Walter Steurer[b]*

[a]FB Chemie, Philipps Universität, 35032 Marburg, Germany, and [b]Laboratory of Crystallography, ETH Zurich, Wolfgang-Pauli-Strasse 10, 8093 Zurich, Switzerland

Correspondence e-mail: steurer@mat.ethz.ch

Received 26 February 2009
Accepted 14 April 2009

This is the second of two papers, where we discuss the cluster structures of a novel family of cluster-based intermetallic phases of unprecedented complexity: $cF444$-$Al_{63.6}Ta_{36.4}$ (AT-19), a = 19.1663 (1) Å, V = 7040 Å^3, $cF(5928 - x)$-$Al_{56.6}Cu_{3.9}Ta_{39.5}$, x = 20 (ACT-45), a = 45.376 (1) Å, V = 93 428 Å^3 and $cF(23, 256 - x)$-$Al_{55.4}Cu_{5.4}Ta_{39.1}$, x = 122 (ACT-71), a = 71.490 (4) Å, V = 365 372 Å^3. The space group is $F\bar{4}3m$ in all three cases. The structures can be described as packings of clusters such as fullerenes, dodecahedra, pentagonal bifrusta and Friauf polyhedra. A characteristic feature of the two larger structures are nets of hexagonal bipyramidal Ta clusters (h.b.p.). The extremely short distance of 2.536–2.562 Å between their apical Ta atoms indicates unusually strong bonding. The large h.b.p. nets are sandwiched between slabs of Friauf polyhedra resembling the structure of the μ phase.

1. Introduction

This is the second of two papers discussing the cluster structures of a novel family of intermetallic phases in the system Al–Cu–Ta (part I: Weber *et al.*, 2009). A cluster-based description of complex crystal structures can be very helpful

Table 1
Description of cluster shells (FK···Frank–Kasper, CN···coordination number).

Cluster shell	No. of faces/vertices	Composition	Remarks
Rhombic dodecahedron	12/14	Al_{14}	First shell of fullerene cluster
Cuboctahedron	14/12	Al_{12}	Second shell of fullerene cluster
CN40 FK polyhedron	76/40	$Al_{12}Ta_{28}$	Second shell of fullerene cluster
Fullerene	40/76	Al_{76}	Third shell of fullerene cluster
Truncated trigonal prism	11/12	$Al_{12}Ta$	Centred by one Ta atom
CN15 FK polyhedron	26/15	$Al_{12}Ta_4$	Centred by one Ta atom
Friauf polyhedron	8/12	$Al_{12}Ta$	Centred by one Ta atom
CN16 FK polyhedron	28/16	$Al_{12}Ta_5$	Centred by one Ta atom
h-Bicapped fullerene	16/28	$Al_{14}Ta_{35}$	Centred by Friauf polyhedron
Dodecahedron	12/20	Ta_{20}	Centred by Al/Cu atoms
Bifrustum	12/15	Ta_{15}	Centred by pentagonal bipyramid of Al atoms
Hexagonal bipyramid (h.b.p.)	12/8	Ta_8	Very short distance between apex atoms

for understanding the geometrical building principles and for identifying hierarchical structures. One has to keep in mind, however, that the term *cluster* does not necessarily imply that these recurrent structural units differ anyhow or anywhere in chemical bonding or stoichiometry from their atomic environment or that they are mechanically particularly stable units (Steurer, 2006; Henley *et al.*, 2006). Large clusters can rather be seen as a kind of (sub)unit cell, which are – similarly to regular unit cells – just structural building blocks. In some cases, however, clusters do represent energetically favourable atomic configurations and their abundance contributes to the stability of these complex structures. *Caveat*: Some seemingly distinct clusters may even be energetically unfavourable arrangements of atoms just needed to fill gaps between energetically favourable clusters.

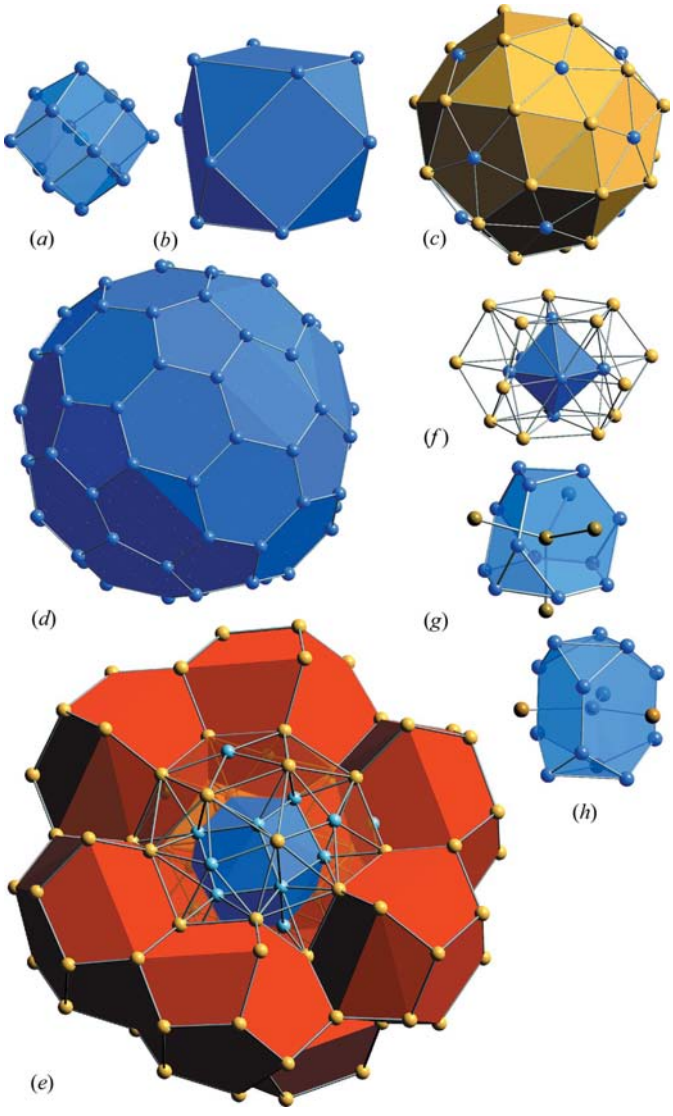

Figure 1
Cluster structures. (*a*)–(*d*) Shells of the fundamental $Al_{102}Ta_{57}$ fullerene cluster (diameter 13.543 Å): (*a*) Al_{14} rhombic dodecahedron around a central Ta atom; (*b*) distorted Al_{12} cuboctahedron merged with a Ta_{28} polyhedron (*c*); (*d*) Al_{76} fullerene shell consisting of 12 *p*(entagons), 28 *h*(exagons) and 76 *v*(ertices); (*e*) partially opened $Al_{102}Ta_{57}$ fullerene cluster with the mantle of bifrusta surrounding cluster (*c*) and centred by cluster (*a*); (f) Al_7Ta_{15} pentagonal Ta_{15} bifrustum around an Al_7 pentagonal bipyramid; (*g*) $Al_{12}Ta_5$ Friauf polyhedron (CN16 FK polyhedron): a truncated Al_{12} tetrahedron centred by a 4-connected Ta atom; (*h*) $Al_{12}Ta_4$ CN15 FK polyhedron: a truncated Al_{12} trigonal prism centred by a 3-connected Ta atom (Al: blue, Ta: brown).

2. Structural description

2.1. Structure of the clusters

The crystal structures of AT-19, ACT-45 and ACT-71 can be described as packings of different subsets of the clusters described in the following (see also Table 1 and Figs. 1, 4, 7 and

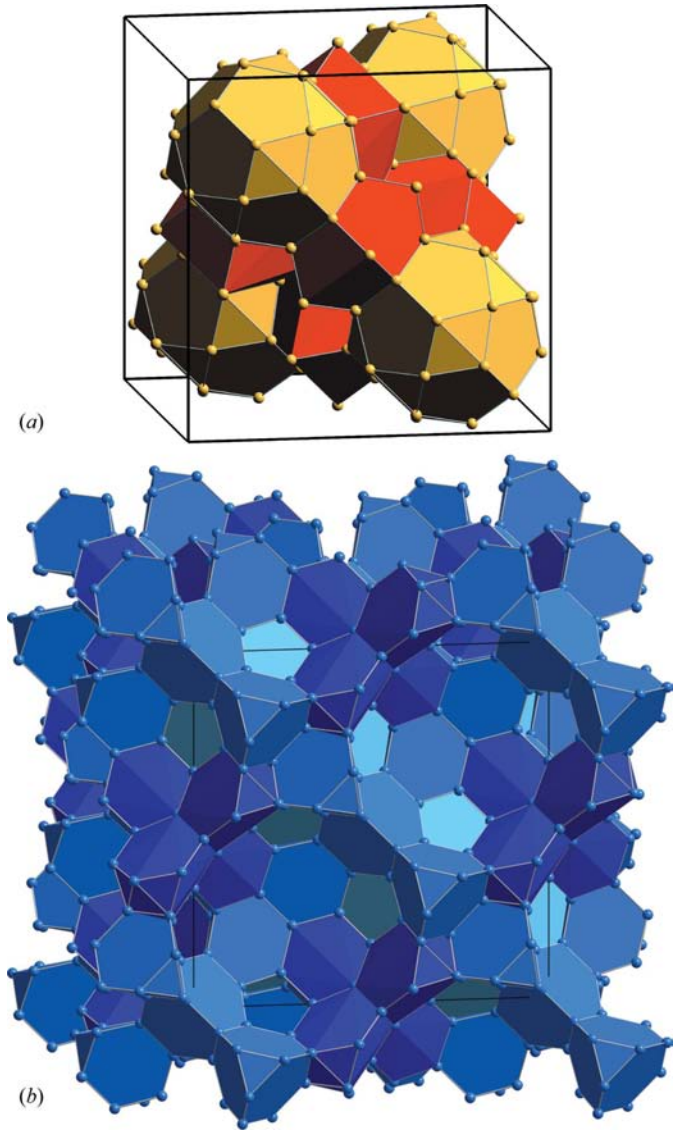

Figure 2
Structure of *cF*444-$Al_{69}Ta_{39}$ (AT-19). The packing of the $Al_{12}Ta_{28}$ cluster shells (see Fig. 1*c*) is shown in (*a*), that of the Al_{76} shells (see Fig. 1*d*) in (*b*). (*a*) The $Al_{12}Ta_{28}$ polyhedra are connected *via* pentagonal Ta bifrusta (red, see Figs. 1*e* and *f*). (*b*) All gaps in the cubic dense packing of Al_{76} fullerenes (light blue) are filled with Friauf (medium blue) and CN15 FK polyhedra (dark blue). The distance between the fullerene cluster centres amounts to 13.543 Å (Al: blue, Ta: brown).

8). There are no 'glue atoms' needed in addition to these clusters to fill space. If there are gaps, for instance, left between densely packed fullerenes, then they are filled by Friauf (CN16) and CN15 (μ phase) Frank–Kasper (FK) polyhedra. The pentagonal bifrusta play a similar role for the gaps in the dodecahedra packings of ACT-45.

(i) $Al_{102}Ta_{57}$ triple-shell fullerene cluster (Figs. 1*a*–*d*), fundamental for all three compounds AT-19, ACT-45 and ACT-71: the first shell around a central Ta atom conforms to an Al_{14} rhombic dodecahedron. Its faces are stellated by Al atoms, which themselves form a tetrahedrally distorted Al_{12} cuboctahedron. The Al atoms at its vertices centre the p(entagonal) faces of a Ta_{28} polyhedron, forming together the second shell, $Al_{12}Ta_{28}$. The symmetry of this FK polyhedron is tetrahedral. The third cluster shell corresponds to an Al_{76} fullerene dual to the $Al_{12}Ta_{28}$ FK polyhedron, with tetrahedral symmetry as well. Each of its h(exagon) faces is bicapped by Ta atoms from the shells below and above. These outermost Ta atoms form the middle Ta_5 rings of pentagonal bifrusta (Figs. 1*e*–*f*). The *p* faces are capped by Al from the second shell.

Generally, fullerenes consist of 12 *p* faces, H *h* faces and V vertices. The number of vertices and faces corresponds to $V = 20 + 2H$ and $F = 12 + H$. Consequently, $H = 28$ for Al_{76}. The limiting polyhedron for $H = 0$ is the pentagonal dodecahedron (Fig. 4*a*).

(ii) Al_7Ta_{15} bifrustum (Fig. 1*f*), abundant in AT-19, ACT-45 and ACT-71: a pentagonal bifrustum consists of two *p* faces and ten trapezoids. The vertices are occupied by Ta atoms and it is centred by a pentagonal bipyramid of Al atoms. This is an essential cluster in all three structures.

(iii) $Al_{12}Ta_5$ Friauf polyhedron (Fig. 1*g*), found in AT-19, ACT-45 and ACT-71: a central Ta atom is surrounded by an Al_{12} truncated tetrahedron. The central Ta atom is linked to four other Ta atoms through the *h* faces. Adding these Ta atoms, which are with ~ 3 Å close to bonding distance, to the coordination polyhedron gives the CN_{16} FK polyhedron. Cu can partially replace Al in this cluster. The Laves phases consist of Friauf polyhedra only.

(iv) $Al_{12}Ta_4$ polyhedron (Fig. 1*h*), found in AT-19: a central Ta atom is surrounded by an Al_{12} truncated trigonal prism. The central Ta atom is linked to three other Ta atoms through the *h* faces. Counting these Ta atoms, which are with ~ 2.9 Å in bonding distance, gives the CN15 FK polyhedron.

(v) $Al_{10}Cu_xTa_{21-x}$ dodecahedron (Fig. 4*a*), found in ACT-45: the Ta_{20} pentagonal dodecahedron is centred by a strongly distorted Al_9 part of an icosahedron. In the type I dodecahedron, one off-centre position is a Ta split site, the other one is a Ta/Cu mixed split position. The dodecahedron of type II, which is interpenetrated by distorted Friauf polyhedra, contains off-centre one Al atom only.

(vi) $Al_{14}Ta_{35}$ *h*-bicapped fullerene (Figs. 4*b* and 6*b* and *c*), found in ACT-45 and ACT-71: the cluster consists of an $Al_{12}Ta$ Friauf polyhedron in the centre surrounded by an Al_2Ta_{26} fullerene ($H = 4$). The *h* faces are

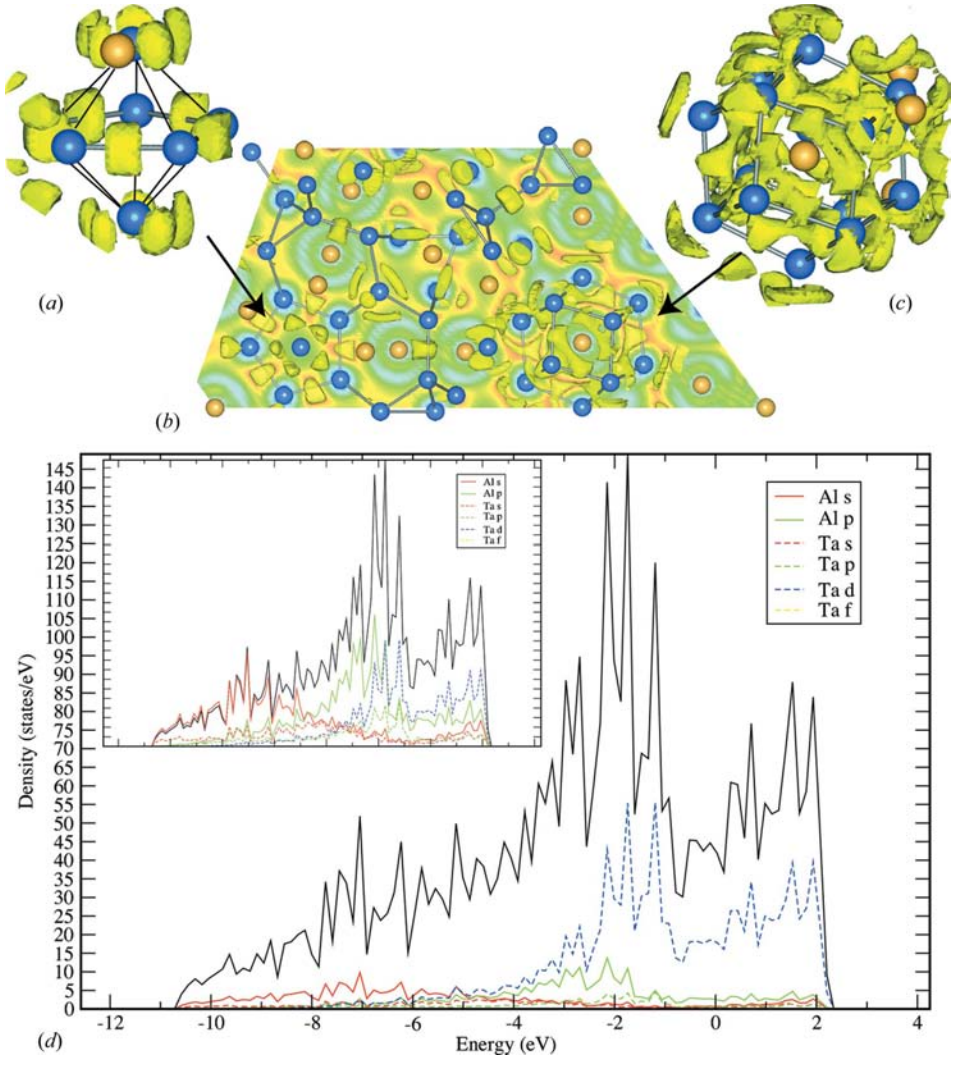

Figure 3
Electron localization function (ELF) of $cF444$-$Al_{63.6}Ta_{36.4}$ (AT-19). The isosurfaces with level 0.65 (max. value is 0.74) are shown as well as a characteristic section (*b*) (blue < green < yellow < red). The pentagonal Al_7 bipyramid inside bifrusta (see Fig. 1*f*) is shown in (*a*) and the Al_{14} rhombic dodecahedron (see Fig. 1*a*), the first shell of the fullerene cluster, in (*c*). (*d*) Electronic density of states (DOS) with five-times exaggerated partial DOS in the inset, with Ta *d* states remaining unscaled (Al: blue, Ta: brown).

bicapped by Ta atoms forming Ta_8 hexagonal bipyramids, h.b.p. (see below).

(vii) $Al_{36}Ta_{81}$ *h*-bicapped fullerene supercluster (Figs. 4*c* and 5*c*), found in ACT-45: four $Al_{14}Ta_{35}$ *h*-capped fullerenes merge into a supercluster centred by a block of five Friauf polyhedra and surrounded by four h.b.p. triples.

(viii) Ta_8 hexagonal bipyramid, h.b.p. (Figs. 4*b* and *c*, 5*c*, 7 and 8), found in ACT-45 and ACT-71: the apex atoms of the hexagonal bipyramid (h.b.p.) have the very short distance of 2.536–2.562 Å. This is the shortest Ta—Ta distance found so far and indicates covalent bonding (Cotton & Hall, 1980). For comparison, the Ta—Ta distance amounts to 2.86 Å in α-Ta, to 2.65 Å in β-Ta (Arakcheeva *et al.*, 2003), to 2.62 Å in β-$Ta_{48}Al_{38}$ (Boulineau *et al.*, 2006) and Ta_6S (Harbrecht, 1988) and to 2.583 Å in the σ phase, *tP*30-$Al_{40}Ta_{60}$ (Boulineau *et al.*, 2006). This cluster, which is the main cluster of the σ phase (Fig. 9), is found in ACT-45 and ACT-71 next to Friauf clusters.

2.2. Structure of AT-19

A new interpretation of the structure of AT-19 (Mahne & Harbrecht, 1994) shows a close relationship to the structures of ACT-45 and ACT-71. It appears to be the simplest representative of this family, just consisting of four $Al_{102}Ta_{57}$ fullerene clusters per unit cell, occupying Wyckoff position $4d\ \frac{3}{4}\frac{3}{4}\frac{3}{4}$.

Each Al_{76} fullerene shell is attached to 12 surrounding ones by sharing the *p* faces. All remaining gaps in this cubic closest packing (c.c.p.) are filled by Friauf and CN15 FK polyhedra (Fig. 2*b*). There are two kinds of tetrahedral voids. One is occupied by just one Friauf polyhedron, the other by a tetrahedral cluster of four CN15 FK polyhedra. The octahedral voids are filled by clusters consisting of five tetrahedrally arranged Friauf polyhedra (as found in α-Mn) plus one CN15 FK polyhedron.

These polyhedra form a D(iamond) net, with the $Al_{102}Ta_{57}$ fullerene clusters filling the open space. Since all *h* faces of the Al_{76} fullerene shell are covered by Friauf or CN15 FK poly-

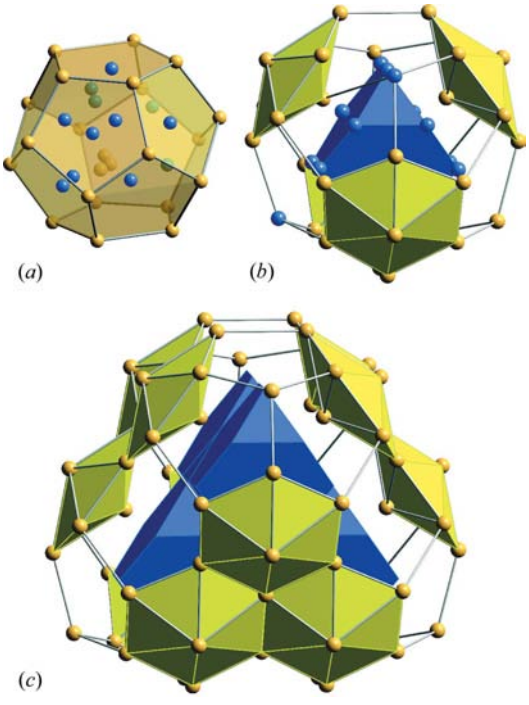

Figure 4
(*a*) $Al_{10}Cu_xTa_{21-x}$ dodecahedron centred by a strongly distorted Al_9 part of an icosahedron; (*b*) $Al_{14}Ta_{35}$ *h*-bicapped fullerene: an Al_2Ta_{26} shell around an $Al_{12}Ta$ Friauf polyhedron (blue), with Ta_8 hexagonal bipyramids (h.b.p.) shaded yellow; (*c*) $Al_{36}Ta_{81}$ supercluster of four interpenetrating $Al_{14}Ta_{35}$ *h*-bicapped fullerenes (Al: blue, Ta: brown).

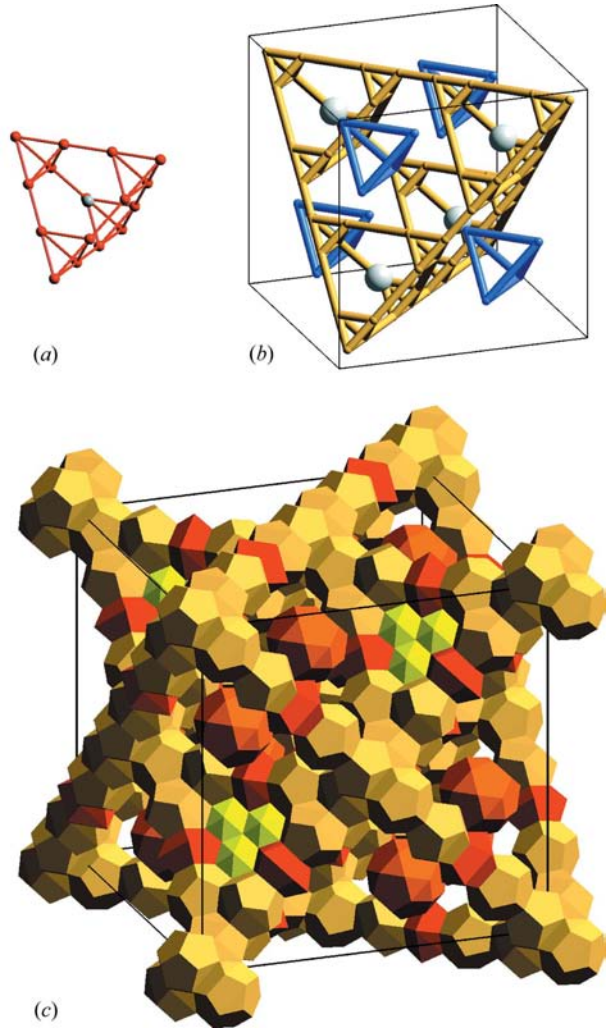

Figure 5
Structural framework of $cF(5928-x)$-$Al_{56.6}Cu_{3.9}Ta_{39.5}$, $x = 20$ (ACT-45). Comparison of (*a*) the network of Cu (red) and Mg (grey) atoms in the cubic Laves phase $MgCu_2$ with (*b*) the network (brown) connecting the centres of $Al_{10}Cu_xTa_{20-x}$ dodecahedra (Fig. 4*a*) and the sites of the $Al_{36}Ta_{81}$ supercluster (Fig. 4*c*) (grey); the $Al_{102}Ta_{57}$ fullerenes (Fig. 1*d*) occupy the vertices of the blue tetrahedra in (*b*). (*c*) Ta framework of the structure: two large interpenetrating tetrahedra, the edges of which are formed by chains of eight dodecahedra and two bifrusta each. The common volume of these two tetrahedra is an octahedron. $Al_{12}Ta_{28}$ fullerene shells (Fig. 1*c*; orange coloured) centre half of the faces of this octahedron and the stellating tetrahedra. The centres of the other half of the stellating tetrahedra are occupied by $Al_{14}Ta_{35}$ *h*-bicapped fullerene superclusters (Fig. 4*c*).

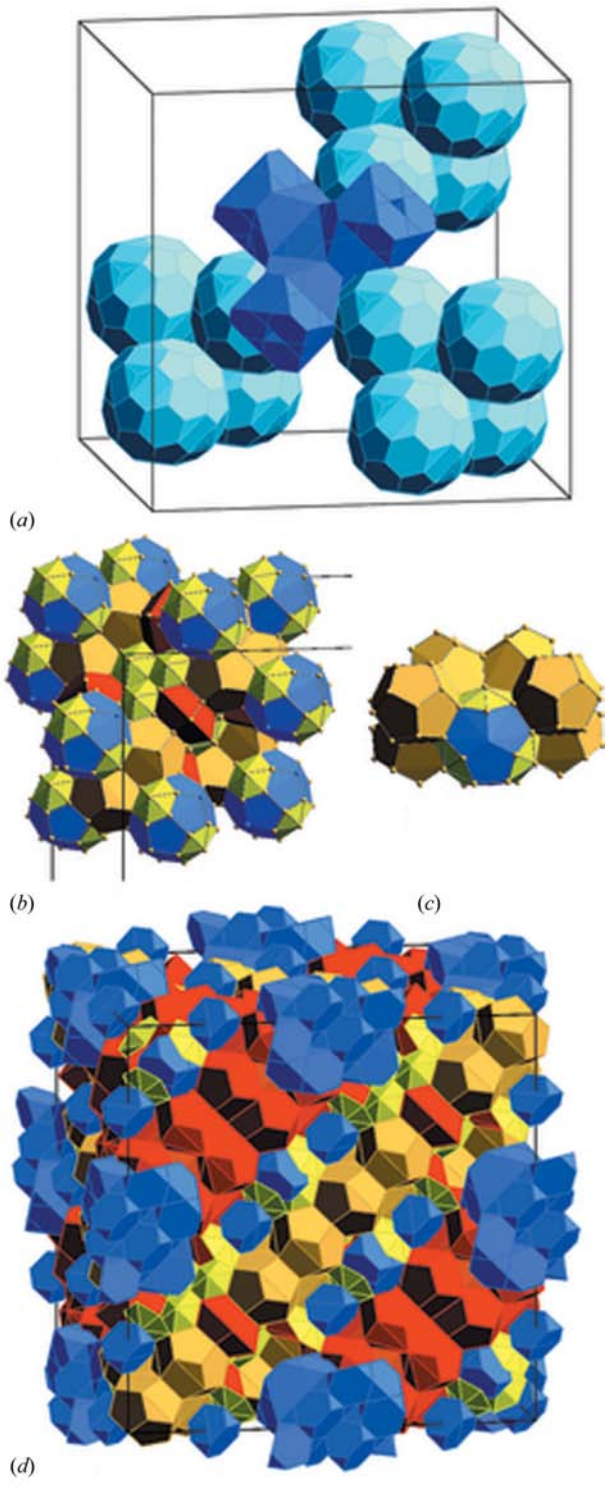

Figure 6
(*a*) Distribution of the $Al_{102}Ta_{57}$ triple-shell fullerene cluster (Figs. 1*a*–*d*) in the unit cell of ACT-45. The four clusters in the upper front have been removed to show the central cluster of 34 Friauf polyhedra 'Laves fragment'. Each fullerene shell shares an *h* face with a Friauf polyhedron of the central Laves fragment. The same cluster is found at the mid-edge positions (*d*). (*b*)–(*c*) The packing of $Al_{10}Cu_xTa_{21-x}$ dodecahedra and $Al_{14}Ta_{35}$ *h*-bicapped fullerenes in the upper left corner of the unit cell. (*d*) Packing of clusters in one unit cell.

hedra, this shell can be seen as just the inside of the D net of Friauf polyhedra. The equatorial pentagons of the bifrusta correspond to the central atoms of the Friauf polyhedra or CN15 FK polyhedra around the *p* faces.

Removing the Al_{76} shells elucidates the role of the bifrusta (Fig. 1*f*), which link, *p*-face sharing, the $Al_{12}Ta_{28}$ shells (Fig. 2*a*). The central Al_5 pentagon of the bifrustum is the joint *p* face of two linked Al_{76} fullerene shells. The bifrusta form a framework with two types of pores. The inner side of one type corresponds to the Ta part of the $Al_{12}Ta_{28}$ shells. The other type of pore has a different shape and contains the nodes of the framework of Friauf and CN15 Frank–Kasper polyhedra.

2.2.1. ELF and DOS. Information about the nature of chemical bonding in a structure can been obtained from the electron localization function (ELF), which reflects the degree of electron localization (*cf.* ELF website: http://www.cpfs.mpg.de/ELF). In an ideal metal, there would not be any ELF maxima between the atoms but only around their centres, reflecting the shell structure of the core electrons. Inspecting the ELF maps of AT-19 (Fig. 3), one finds the strongest maxima between the Al atoms of the 5-rings centring the pentagonal bifrusta (Figs. 3*a* and 1*f*). The resulting strong bonding is reflected in the short Al—Al distances, which are in the range 2.398–2.557 Å (2.517–2.562 Å in the fully relaxed structure; relaxed means that the self-consistent energy steps converged below 10^{-4} eV after allowing all atoms to move).

The Al atoms of the rhombic dodecahedron, *i.e.* the first shell of the fullerene cluster, appear quite strongly bonded to each other with distances 2.477–2.579 Å (2.635–2.649 Å in the relaxed structure), and to some extent to the central Ta atom as well (Figs. 3*c* and 1*a*). There are no indications for covalent Ta—Ta bonds in AT-19 contrary to ACT-45 and ACT-71, where the short distances between the apical Ta atoms in the h.b.p. indicate covalent bonding. The ELF calculations shown in Fig. 3 have been performed with all sites of the rhombic dodecahedron fully occupied, *i.e.* for a composition $Al_{72}Ta_{39}$, as is the case for ACT-45. In the case of ACT-71, some of the vertices of the inscribed cube are only partially occupied ($\sim$ 70%), while in the case of AT-19, these vertices are fully occupied and the other six Al atoms split.

From the viewpoint of chemical bonding, there are only two kinds of clusters left, which can be considered as special entities. These are the bifrusta, particularly the Al_5 rings, and the rhombic dodecahedron. Consequently, one can conclude that in AT-19 there is a metallically bonded framework of Friauf and CN15 polyhedra, which largely interpenetrates a framework of partially covalently bonded bifrusta. The empty space left is occupied by more covalently bonded rhombic dodecahedra.

The calculations have been performed with the *VASP* (Vienna *ab initio* simulation package) code (Kresse & Furthmuller, 1996*a*,*b*). The generalized gradient approximation (GGA; Perdew *et al.*, 1996) together with the projector-augmented wave (Blochl, 1994) method has been used to optimize the structure and calculate the charge distribution at 0 K. In all calculations the projector-augmented wave (PAW) potentials and a $4 \times 4 \times 4$ Monkhorst–Pack scheme

(Monkhorst & Pack, 1976) for the Brillouin zone sampling, as provided by the code, were used. The positions of all atoms were relaxed with the conjugate gradient method. The electron localization function (ELF, η) was calculated with the ELF module provided with the VASP code. For an overview see the ELF website (http://www.cpfs.mpg.de/ELF).

2.3. Structure of ACT-45

The structure of ACT-45 can be seen as a packing of tetrahedral superclusters of four $Al_{102}Ta_{57}$ fullerenes, of Friauf polyhedra, pentagonal dodecahedra, bifrusta, *h*-capped fullerenes and $Al_{36}Ta_{81}$ superclusters (Figs. 5 and 6).

The framework of the structure is built from chains of pentagonal dodecahedra and bifrusta (Fig. 5). These chains form two large interpenetrating tetrahedra, which can also be described as stellated octahedra, stella octangula. Besides single *h*-capped fullerenes, which are surrounded by dodecagons, $Al_{36}Ta_{81}$ superclusters are also found sharing their *p* faces with dodecahedra. Bifrusta fit into the reentrant parts of the supercluster.

Half of the outer star tetrahedra are filled with $Al_{36}Ta_{81}$ superclusters (Fig. 5*c*). The other four star tetrahedra each contain a supercluster of four $Al_{102}Ta_{57}$ fullerene clusters, *i.e.* exactly one unit cell of AT-19 (Fig. 2). Each fullerene centres one of the faces of a star tetrahedron and thereby also the faces of a central octahedron. The centre of the octahedron and the symmetrically equivalent mid-edge positions are occupied by a block of 58 Friauf polyhedra, later on called 'Laves fragments', surrounded by four $Al_{102}Ta_{57}$ fullerenes (Fig. 6*a*). Each fullerene cluster shares an *h* face with the central 'Laves fragment'.

There are two kinds of pentagonal dodecahedra. Around the origin, four face-sharing dodecahedra of type I form a tetrahedral cluster (Fig. 6*b*). The Ta atoms at the vertices, where three dodecahedra meet, centre Friauf polyhedra. Nine of the 12 Al atoms at the vertices of Friauf polyhedra are located inside each dodecahedron. There is, furthermore, one triply split Ta atom as well as a mixed Cu/Ta triply split position. The dodecahedra of type II are partially surrounded by bifrusta. Instead of the Cu/Ta triply split position they contain just an Al atom.

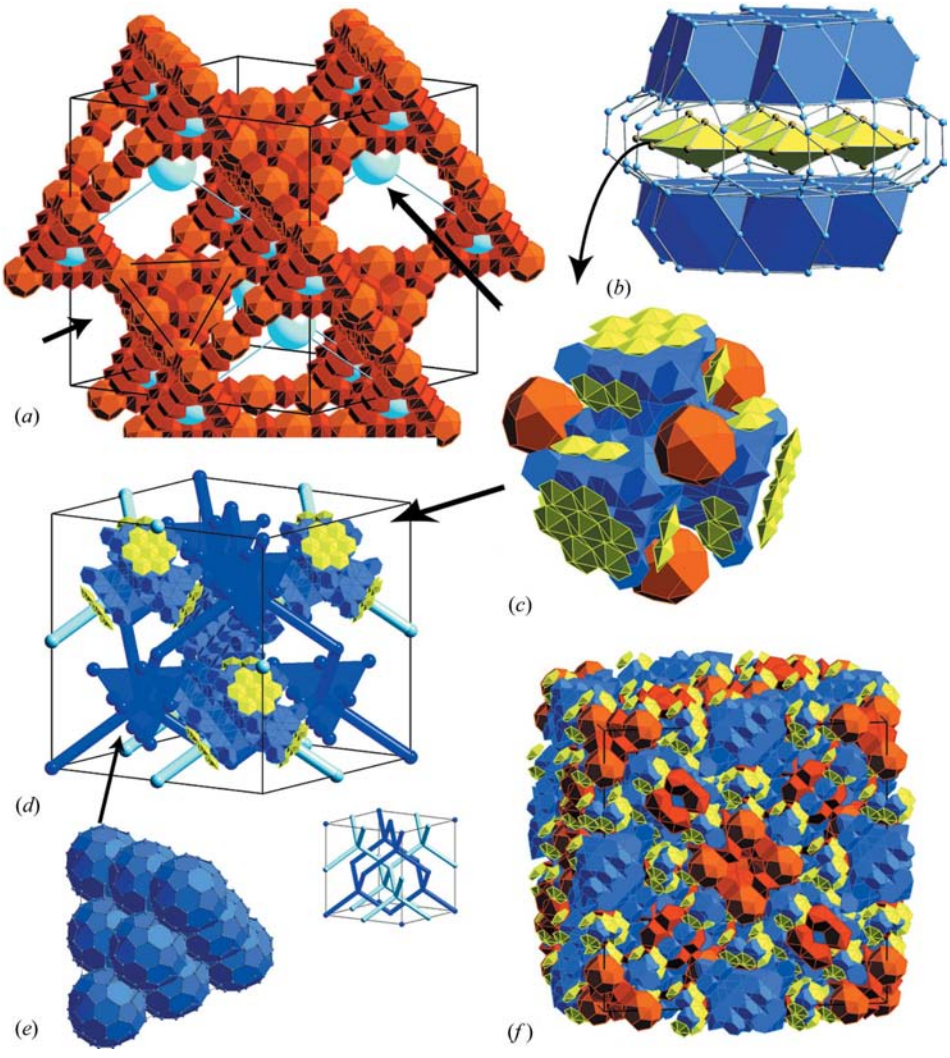

Figure 7
Structural building principle of $cF(23\,256 - x)$-$Al_{55.4}Cu_{5.4}Ta_{39.1}$, $x = 122$ (ACT-71). (*a*) Framework of $Al_{12}Ta_{28}$ fullerene shells (orange) linked by bifrusta (red). Left: one tetrahedral supercluster of ten fullerenes is outlined in black and marked by an arrow. The big light-blue spheres mark the positions of the 'Laves blocks' (*c*) and (*d*). (*b*) h.b.p. 7-net sandwiched by slabs of Friauf clusters from adjacent 'Laves blocks'. (*c*) 'Laves block' consisting of 146 Friauf polyhedra with h.b.p. and $Al_{12}Ta_{28}$ fullerene shells. The Al_{76} shells (not shown) share *h* faces with the 'Laves block'. The corners, face centres and one half of the eighth cubes of the unit cell (*d*) are occupied by tetrahedral superclusters of each ten $Al_{102}Ta_{57}$ fullerenes (in total 80) (*e*). The centres of the fullerenes are marked by small dark-blue spheres. (*f*) One unit cell of ACT-71.

2.4. Structure of ACT-71

The structure of ACT-71 can be described as the packing of eight tetrahedral superclusters, consisting each of ten $Al_{102}Ta_{57}$ fullerenes (Fig. 7*e*), eight blocks of 146 Friauf polyhedra, later on called 'Laves blocks' (Fig. 7*c*) as well as of bifrusta, *h*-capped fullerenes and h.b.p. 7-nets (six h.b.p. condensed to a central h.b.p.). The fullerene superclusters occupy the sites 4*a* (0 0 0) and 4*c* ($\frac{1}{4}$ $\frac{1}{4}$ $\frac{1}{4}$) of a double-diamond type structure (*cF*16-NaTl type), while the 'Laves blocks' are centred at the sites 4*b* ($\frac{1}{2}$ $\frac{1}{2}$ $\frac{1}{2}$) and 4*d* ($\frac{3}{4}$ $\frac{3}{4}$ $\frac{3}{4}$)

(Fig. 7*d*). If the equivalent sites in such a double-diamond structure are connected, two interwoven D nets are formed. The distances between equivalent sites on such a D net are $a(3^{1/2})/4$ = 30.956 Å and between sites of different D nets 35.745 Å.

The central part of a 'Laves block' consists of a tetrahedral cluster of 30 Friauf polyhedra with the structure of the cubic Laves phase. On top of each tetrahedron face of this cluster, there are 29 Friauf polyhedra assembled in two slabs with the structure of the hexagonal Laves phase.

From a geometrical point of view, the size of the unit cell is controlled by the dimensions of the framework of Al_2Ta_{26} fullerene shells and bifrusta (Fig. 7*a*). It consists of small- and medium-sized tetrahedra attached to truncated large tetrahedra. This arrangement corresponds to the network spanned by the Cu atoms of the cubic Laves phase. The space inside

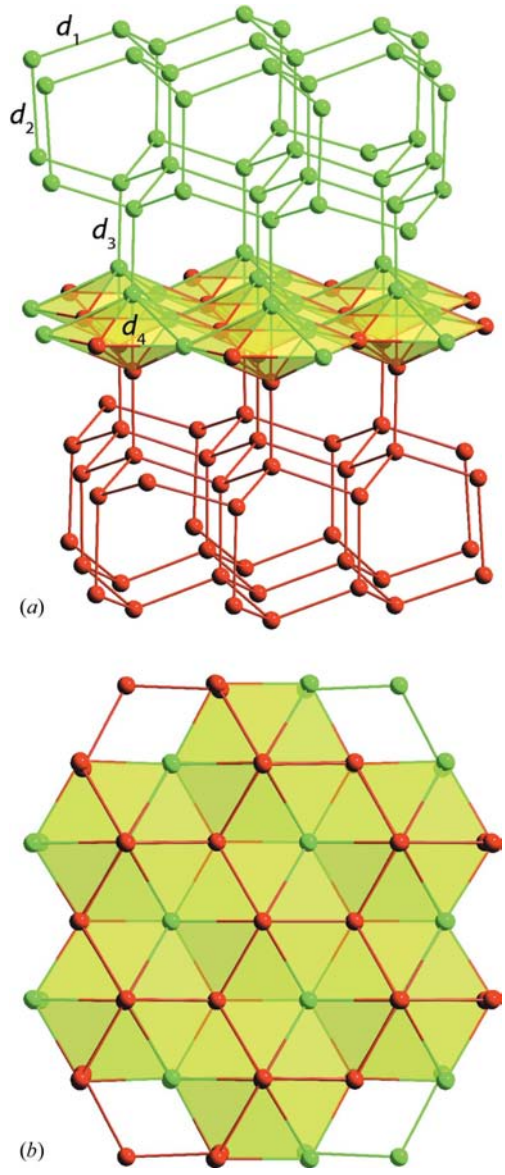

Figure 8
Ta skeleton of an h.b.p. 7-net sandwiched by Friauf polyhedra. (*a*) Perspective view of the Ta skeleton of the structure part shown in Fig. 7(*b*) and (*b*) its projection onto the h.b.p. layer. Upper and lower Ta skeletons are coloured differently to show that h.b.p. are formed by 4-connected Ta from slabs of Friauf polyhedra that are shifted by $\frac{1}{2}\,\frac{1}{2}\,0$ (in units of hexagon edges) against each other [green vertices into the centres of red hexagons in (*b*)]. The Ta skeleton is a 4-connected net of the lonsdaleite type, *i.e.* it contains skew hexagons in both chair and boat conformations. The bond lengths amount to: d_1 = 3.053–3.108 (3.067–3.101), d_2 = 3.092–3.294 (3.076–3.282), d_3 = 2.836–2.878 (2.859–2.892), d_4 = 2.536–2.562 Å. The numbers in parentheses refer to the equivalent bonds marked in red.

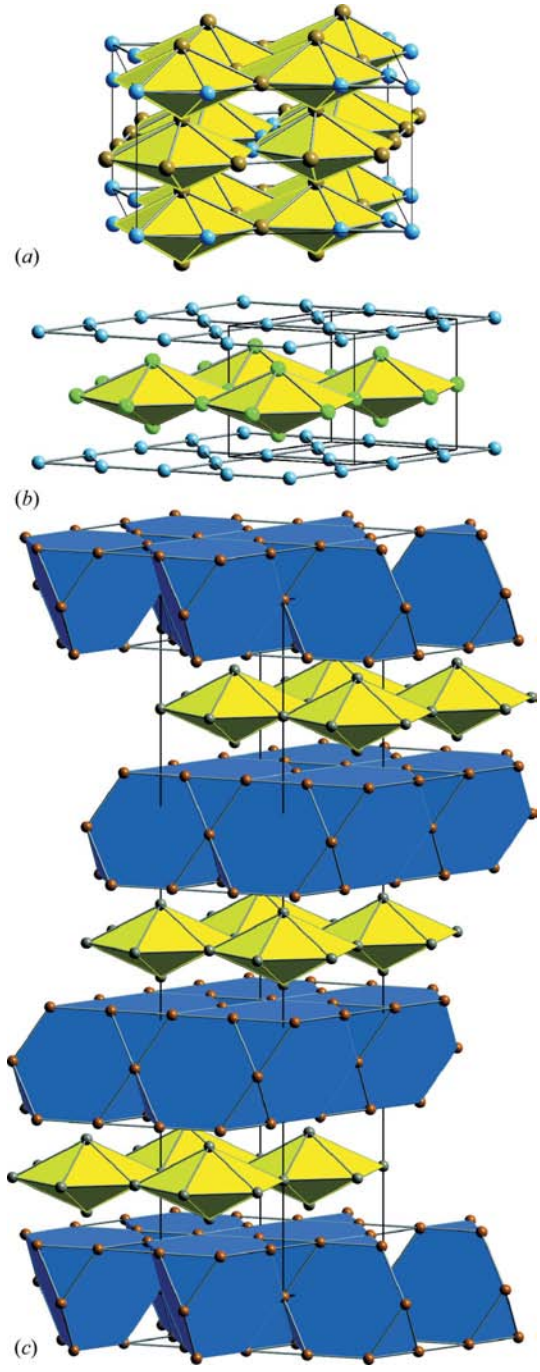

Figure 9
Illustration of the cluster structures of (*a*) the σ phase *tP*30-$Al_{40}Ta_{60}$, (*b*) *hP*7-Al_3Zr_4, and (*c*) the μ phase *hR*13-Fe_7W_6. In all three cases, CN12, CN14 and CN15 FK polyhedra could be used for the cluster representation instead of h.b.p. The unit cells are marked by black lines.

each of these small tetrahedra is filled by a Laves block (marked by light blue spheres in Fig. 7*d*). The medium-sized tetrahedra are just the fullerene superclusters (marked by an arrow in Fig. 7*a*). The large pores in this framework, *i.e.* the large truncated tetrahedra, are occupied each by a 'Laves block' and two fullerene superclusters.

Owing to the constraints applied by this framework, the 'Laves blocks', occupying the vertices on one D net, meet each other with a stacking fault, *i.e.* a flat layer of seven h.b.p. (Figs. 7*b–d* and 8). The h.b.p. layers consist entirely of Ta atoms, contrary to those in the σ phase *tP*30-$Al_{40}Ta_{60}$, where almost all sites are to some extent Al/Ta mixed positions (Fig. 9*a*). The Ta—Ta distances (d_3) to the h.b.p. net are significantly shorter (< 2.9 Å) than those (d_1, d_2) connecting the Ta atoms inside the Laves block (> 3 Å) (Fig. 6*a*) and comparable to the bond lengths in α-Ta. Furthermore, as in the case of ACT-45, the apical Ta—Ta distances (d_4) in the h.b.p. layers are at 2.536–2.562 Å the shortest known, indicating strong bonding. There are no Al—Al bonds reaching through these h.b.p. layers. The h.b.p. layer together with the neighbouring Al Kagomé layers form a slab of seven unit cells of the *hP*7-Al_3Zr_4 structure (Fig. 9*b*). This layer also resembles the structure of the μ phase *hR*13-$(Al,Cu)_{53.8}Ta_{46.2}$ (Fig. 9*c*). A smaller variant of a similar interface, corresponding to just one Al_3Zr_4 unit, has been reported for *cF*1192-$NaCd_2$ (Fredrickson *et al.*, 2007).

3. Conclusions

Where are the Cu atoms in ACT-45 and ACT-71? Cu mainly substitutes for Al at the boundaries between Friauf polyhedra and Al_{76} fullerene shells. The substitution of Al by Cu changes the electron concentration. The repulsion between Cu and Ta atoms is favourable for a separation of (Al,Cu)-rich and Ta-rich parts of the structure. Indeed, the structure contains (Al,Cu)-poorer parts consisting of fullerene superclusters, with composition $(Al,Cu)_{1.8}Ta$, and (Al,Cu)-richer parts represented by the Laves blocks, with composition $(Al,Cu)_2Ta$. Both parts are interwoven with each other along the D nets.

In summary, ACT-45 and ACT-71 can be seen as a compromise between AT-19, the σ phase, the μ phase and the hexagonal Laves phase. The Laves phase ($Al_{57.4}Cu_{9.3}Ta_{33.3}$) has the lowest Ta content, followed by AT-19 ($Al_{63.6}Ta_{36.4}$), ACT-71 ($Al_{55.4}Cu_{5.4}Ta_{39.2}$), ACT-45 ($Al_{56.6}Cu_{3.9}Ta_{39.5}$), the μ phase [$(Al,Cu)_{53.8}Ta_{46.2}$] and finally the σ phase ($Al_{40}Ta_{60}$). Formally, adding Ta to the Laves phase results in its fragmentation and in the formation of fullerene clusters as well as of h.b.p. layers for adapting the Laves block mismatch and restoring the average stoichiometry.

References

Arakcheeva, A., Chapuis, G., Birkedal, H., Pattison, P. & Grinevitch, V. (2003). *Acta Cryst.* B**59**, 324–336.

Blochl, P. E. (1994). *Phys. Rev. B*, **50**, 17953–17979.

Boulineau, A., Joubert, J.-M. & Černý, R. J. (2006). *Solid State Chem.* **179**, 3385–3393.

Cotton, F. A. & Hall, W. T. (1980). *Inorg. Chem.* **19**, 2354–2356.

Fredrickson, D. C., Lee, S. & Hoffmann, R. (2007). *Angew. Chem. Int. Ed.* **46**, 1958–1976.

Harbrecht, B. (1988). *J. Less Common Met.* **138**, 225–234.

Henley, C. L., De Boissieu, M. & Steurer, W. (2006). *Philos. Mag.* **86**, 1131–1151.

Kresse, G. & Furthmuller, J. (1996*a*). *Comput. Mater. Sci.* **6**, 15–50.

Kresse, G. & Furthmuller, J. (1996*b*). *J. Phys. Rev. B*, **54**, 11169–11186.

Mahne, S. & Harbrecht, B. (1994). *J. Alloys Comp.* **203**, 271–279.

Monkhorst, H. J. & Pack, J. D. (1976). *Phys. Rev. B*, **13**, 5188–5192.

Perdew, J. P., Burke, K. & Ernzerhof, M. (1996). *Phys. Rev. Lett.* **77**, 3865–3868.

Steurer, W. (2006). *Philos. Mag.* **86**, 1105–1113.

Weber, T., Dshemuchadse, J., Kobas, M., Conrad, M., Harbrecht, B. & Steurer, W. (2009). *Acta Cryst.* B**65**, 308–317.